

See discussions, stats, and author profiles for this publication at: <https://www.researchgate.net/publication/346013185>

Wireless Power Transfer Approaches for Medical Implants: A Review

Article · December 2020

DOI: 10.3390/signals1020012

CITATIONS

43

READS

2,275

2 authors:



Mohammad Haerinia
University of Massachusetts Lowell

33 PUBLICATIONS 208 CITATIONS

[SEE PROFILE](#)



Reem Shadid
Applied Science Private University

17 PUBLICATIONS 187 CITATIONS

[SEE PROFILE](#)

Some of the authors of this publication are also working on these related projects:




Wireless Power Transfer for Biomedical Applications [View project](#)



Wireless power transfer [View project](#)

Review

Wireless Power Transfer Approaches for Medical Implants: A Review

Mohammad Haerinia ^{1,*}  and Reem Shadid ²

¹ School of Electrical Engineering and Computer Science, University of North Dakota, Grand Forks, ND 58202, USA

² School of Electrical Engineering Department, Applied Science Private University, Amman 11931, Jordan; re_shadid@asu.edu.jo

* Correspondence: mohammad.haerinia@und.edu

Received: 6 September 2020; Accepted: 10 November 2020; Published: 16 December 2020



Abstract: Wireless power transmission (WPT) is a critical technology that provides an alternative for wireless power and communication with implantable medical devices (IMDs). This article provides a study concentrating on popular WPT techniques for IMDs including inductive coupling, microwave, ultrasound, and hybrid wireless power transmission (HWPT) systems. Moreover, an overview of the major works is analyzed with a comparison of the symmetric and asymmetric design elements, operating frequency, distance, efficiency, and harvested power. In general, with respect to the operating frequency, it is concluded that the ultrasound-based and inductive-based WPTs have a low operating frequency of less than 50 MHz, whereas the microwave-based WPT works at a higher frequency. Moreover, it can be seen that most of the implanted receiver's dimension is less than 30 mm for all the WPT-based methods. Furthermore, the HWPT system has a larger receiver size compared to the other methods used. In terms of efficiency, the maximum power transfer efficiency is conducted via inductive-based WPT at 95%, compared to the achievable frequencies of 78%, 50%, and 17% for microwave-based, ultrasound-based, and hybrid WPT, respectively. In general, the inductive coupling tactic is mostly employed for transmission of energy to neuro-stimulators, and the ultrasonic method is used for deep-seated implants.

Keywords: wireless power transfer; implanted device; inductive link; microwave link; ultrasound link; hybrid link

1. Introduction

In recent years, medical progress has evolved with an increased interest in instruments for sensing and controlling the specific functions of the brain. These medical instruments considerably decrease morbidity and improve the standard of life for certain patients. Sensor systems are now quite advanced but providing power to these devices is still a major challenge. The answer to this issue is using wireless power transmission (WPT) technologies for a range of biomedical implants. WPT is a secure and appropriate energy supply for recharging biosensors and electrical implanted devices as well as for data communication in these specific applications.

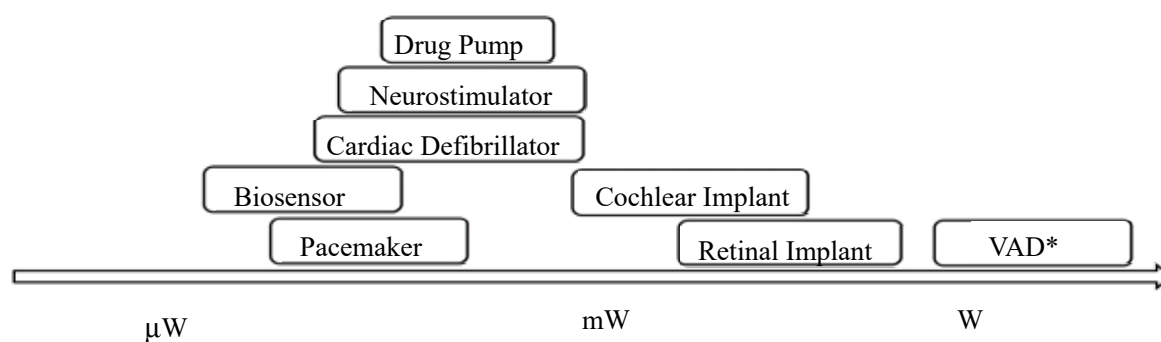
WPT comprises two main methods: near-field and far-field transmission. The region is considered near-field if it satisfies two conditions: First, the distance between the transmitter and receiver coil (d) should be less than one wavelength (λ) at the operating frequency ($d < \lambda$), and second, the largest dimension of the transmitter coil (D) should be less than $\lambda/2$. In contrast, for far-field $D > \lambda/2$. Moreover, the near and far fields are defined in terms of the Fraunhofer distance ($d_F = 2D^2/\lambda$); if the conditions $d_F \gg D$ and $d_F \gg \lambda$ are satisfied, the region is considered far-field.

There are three major ways to accomplish a near-field WPT: (1) capacitive coupling based on electric fields; (2) inductive coupling based on magnetic fields; and (3) magnetic resonant inductive coupling, which include a resonant circuit in transmitter and receiver coils. Far-field WPT is also known as microwave coupling. Hybrid wireless power transmission (HWPT) includes both far-field and near-field WPT.

The biomedical implants are intended to be used for biological studies, therapy, and medical diagnostics. Novel biological materials also provide additional biocompatibility and efficiency, as well as reduced expenses. Implantable medical devices (IMDs) can be classified into two primary categories based on their methodologies for the transmission of power. Transfer mechanisms such as inductive coupling, optical charging, and ultrasound are included in the first category. The second category is split into two subsections: batteries, such as lithium; and natural harvesting, including biofuel cell, thermoelectricity, piezoelectricity, electrostatic, and electromagnetic [1]. Various WPT techniques are reviewed in the literature. For instance, the ultrasound and inductive coupling methods were evaluated by Taalla et al. [2] and Shadid et al. [3], respectively. In this paper, common WPT approaches for IMDs, including inductive coupling, microwave, and ultrasound, are studied. HWPT systems, a mixture of two different methods, are also reviewed.

2. Different Approaches for a Wireless Power Transfer System

The lifespan of IMDs is limited to battery capabilities. Patient pain and the danger of infection are the major development concerns in implantable medical systems because using implanted batteries can cause diseases [4]. Therefore, the WPT link is a safer option to power biomedical implants [4]. Improving WPT techniques and efficiency will enable rechargeable batteries to be employed for IMDs rather than non-rechargeable batteries, which usually have a greater weight and volume and a shorter period of effectiveness compared to rechargeable batteries. Medical implants like implanted spinal cord stimulators can use a rechargeable battery to improve their capability and reduce overall costs [5]. Lately, there has been a great interest in the usage of WPT for medical applications. The development of implantable electronic devices in biological systems has made it easier to use this technology for powering various IMDs, such as biological sensors, pacemakers, and neurostimulator, working in a range of power from a few microwatts to a few watts. In Figure 1, the power ranges of common IMDs are illustrated [1,6]. The WPT systems for the neurostimulator and the pacemaker are discussed in detail in [7–13].



*Ventricular Assist Device

Figure 1. Power ranges of implantable medical devices (IMDs).

There are reliability problems with the classic wireless power links. An option that facilitates the growth of a number of bio-implants is the use of CMOS processes. In this procedure, the standard CMOS is included with the implanted receiver. This reduces the cost, improves productivity, and provides compatibility and reliability of prototypes [14,15]. The usage of CMOS for WPT systems is presented in [15–23]. A backward communication unit transmits the information to an external data communicator using modulation. Typically, FSK [24], PSK [25], ASK [26], OOK [27], LSK [28], PPSK [29],

QMPM [30], QPSK [31], and impedance modulation [32] have been used for data communication units in medical applications. Long-term RF and microwave exposure are dangerous. The device layout must comply with the associated safety regulations to protect patients from electromagnetic radiation damage. It is possible to evaluate maximum permissible exposure (MPE) in environments for electromagnetic field intensity by assessing the specific absorption rate (SAR). IEEE Standard Basis C95.1 expresses SAR limitation. According to IEEE 1992 standard, the maximum SAR value must be below 1.6 W/kg for any 1 g of the body tissue and below 0.08 W/kg for the whole body. Nevertheless, the maximum SAR limitation is 4 W/kg for every 10 g of tissue of body parts such as hands, feet, ankles, and wrists, as per IEEE 2005 standard.

The authors proposed an arrangement to decrease the SAR and improve safety for inductive WPT systems [33]. They designed a multi-transmitter configuration consisting of an array of symmetric resonant elements. The array will significantly decrease the amount of electric field generated by the fed loop and thus reduce the electromagnetic exposure of the biological tissues.

Mainly, determining SAR can be achieved by using numerical techniques and empirical models using fabricated tissue phantoms [4,34–38]. In [39], the body tissue was used as the power transfer channel. According to this technique, medical electrodes are attached on the body surface to supply power to a miniaturized implant with a differential input. The maximum SAR value was studied in [40,41]. The empirical results can be obtained in vivo [8,42,43], using a living organism, or in vitro [44–46], outside of a living organism. To mimic the biological effects of human body tissue, the phantom is very popular among researchers in this field. The material type and amount needed for muscle phantom fabrication is summarized and measured in [47]. The tissue’s electromagnetic properties play an important role in the design of implantable devices. An assessment of variation in tissue electromagnetic properties was provided by Bocan et al. [48]. The recent reports on tissue electromagnetic properties are depicted in Table 1.

Table 1. Summary of different approaches in analyzing tissue electromagnetic properties.

Reference	Year	Tissue	Frequencies	Models/Methods
[49]	2020	In vivo, ex vivo	-	FEM *
[50]	2019	Muscle, fat, skin	50 MHz, 300 MHz, 700 MHz, and 900 MHz	FDTD **
[51]	2019	Body	(0.5–26.5) GHz	Measured properties, Cole–Cole
[52]	2018	Brain, liver	200–1600 Hz	Measured properties
[53]	2018	Muscle, fat, skin	915 MHz and 2 GHz	Measured properties
[54]	2017	Blood, liver, fat, brain	10 kHz–10 MHz	Bottcher–Bordewijk model, measured properties
[55]	2016	Muscle, bladder, cervix	128 MHz	Measured properties, Cole–Cole
[56]	2016	Body/14 tissues	2.1 GHz, 2.6 GHz	FDTD
[57]	2016	Head	(0.75–2.55) GHz	Phantom/ FEM
[58]	2016	Muscle	500 MHz–20 GHz	Fricke
[59]	2015	Eye/6 tissues	(0.9–10) GHz	FDTD
[60]	2015	Skin	(0.8–1.2) THz	FEM
[61]	2014	Eye, head/14 tissues	(0.9–5.8) GHz	FDTD
[62]	2010	Head	-	FEM
[63]	2009	Head/16 tissues	50 MHz–20 GHz	Measured properties, FDTD
[64]	2006	Eye, head/15 tissues	900 MHz, 1800 MHz, 2450 MHz	FDTD
[65]	2004	Body	400 MHz, 900 MHz, 2400 MHz	Visible human, FDTD
[66]	2004	Body/51 tissues	30 MHz–3 GHz	FDTD
[67]	2002	Head/10 tissues	900 MHz, 1800 MHz	Visible human, FDTD

* Finite element method. ** Finite-difference time-domain.

2.1. Inductive-Based Wireless Power Transfer

Inductive coupling is the process of transferring power by connecting a source that is generating a varying magnetic field to a primary coil which is usually located outside the body tissue. Then, based on Faraday’s law, the voltage is induced across the receiver secondary coil, which is usually implanted inside the body tissues. Figure 2 below illustrates this principle.

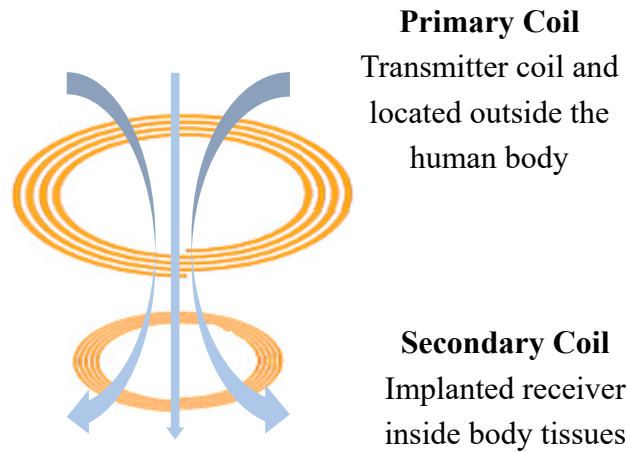


Figure 2. Inductive coupling principle.

The amount of induced voltage in implanted coils (V_{is}) is given by the following equation

$$V_{is} = -N \frac{d\Phi}{dt} = jN\omega\Phi = jN\omega\mu \int \vec{H} \cdot d\vec{s} \tag{1}$$

where N is the number of turns, ω is the operating angular frequency, Φ is the magnetic flux linkage, and μ is the permeability of transfer medium. According to Equation (1), coupling between coils depends mainly on the amount of Φ between the primary (transmitter) and secondary (implanted) coils. Thus, when the distance between the transmitter and the implanted receiver is decreased the amount of coupled magnetic flux will increase.

Furthermore, the amount of transferred power using inductive coupling could be increased by adding a capacitor for resonance. The simplified diagram of the resonant inductive WPT circuit is shown in Figure 3. L_1 is the transmitter coil inductor that is located outside the body tissues, and L_2 is the implanted receiver coil inductor, often with the rest of the implant electronics. Coil windings have parasitic capacitance and resistance associated with them, which are shown as symmetric elements (R_{s1}, R_{s2}), and (C_{s1}, C_{s2}). Capacitors C_T and C_R are added to the circuit to form an LC resonance with L_1 and L_2 , respectively. R_L is the load resistance.

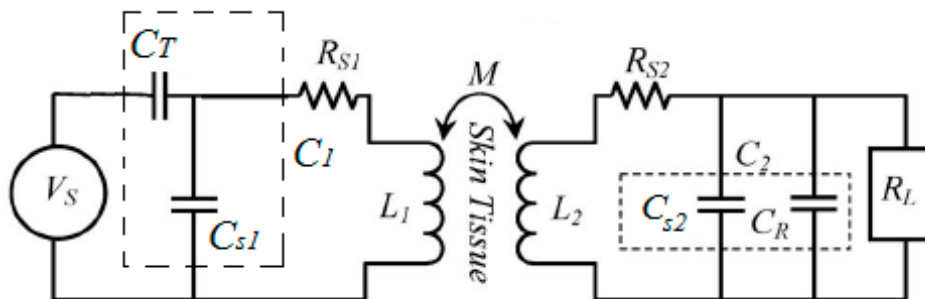


Figure 3. Circuit model of magnetic resonant inductive coupling.

The highest efficiency and voltage gain are achieved when both LC tanks are tuned at the operating frequency of the link $\omega_o = 1/\sqrt{L_1C_1} = 1/\sqrt{L_2C_2}$, where C_1 and C_2 are a combination of the lumped capacitor and the parasitic capacitance of the transmitter and implanted coils, respectively.

The delivered power is transferred between the transmitter and the implanted coils through mutual inductance (M). M is related to the coupling coefficient (k) according to

$$k = \frac{M}{\sqrt{L_1L_2}} \quad (2)$$

The quality factors for the transmitter (Q_1), receiver (Q_2), and load (Q_L) circuits are calculated as follows:

$$Q_1 = \frac{\omega_o L_1}{R_{s1}}, \quad Q_2 = \frac{\omega_o L_2}{R_{s2}}, \quad Q_L = \frac{R_L}{\omega_o L_2} \quad (3)$$

The total efficiency, η_{ind} , is calculated according to Equation (4), as derived in [3]:

$$\eta_{ind} = \frac{k^2 Q_1 Q_2}{1 + k^2 Q_1 Q_2 + \frac{Q_2}{Q_L}} \times \frac{1}{1 + \frac{Q_L}{Q_2}} \quad (4)$$

More details on how to derive the efficiency of inductive links can be found in [68]. In general, the efficiency increases at high delivered power. However, different efficiencies have been achieved for the same transmitted power depending on the system design. Inductive coupling is a common and efficient way to transfer data and power into implantable medical instruments, including cardiac pacemakers, implantable cardioverter defibrillators, recording devices, neuromuscular stimulators, and cochlear and retinal implants.

When the development of an inductive link using a power amplifier is applied, the output power depends on the operating frequency and the distance range. The bandwidth to support data communication and reasonable efficacy for power transfer, insensitivity to misalignments, and biocompatibility are needed for a robust inductive link for medical implants [69]. In general, hundreds of kilohertz to a few megahertz is the operating frequency, and the size of the implanted coil is between several millimeters and a few centimeters. As the frequency increases, the electromagnetic wavelength becomes more commensurate with the coil dimension and the space between the coils. In this stance, the radiative and non-radiative components are part of the electromagnetic waves. Biological tissue also creates significant problems for the propagation of electromagnetic fields and dilutes the electrical field, thus affecting the efficiency of the inductive link [33]. According to Faraday's induction law, increasing the size of coils and the number of turns boosts inductive link efficiency [33]. When the transmitting coil and the receiving coil have the same size, the maximum coupling is achievable. Although, in practice, the implanted coil is significantly smaller than the transmitting coil [70]. Mainly, the inductive-based WPT system is used for medical devices such as brain and spinal cord stimulators. Lyu et al. [8] have developed a stimulator that occupies an area of 5 mm × 7.5 mm and operates at the resonant frequency of 198 MHz while having a 14 cm distance from the transmitter, which is located outside of the body. The stimulator gets the energy that has already been stored by a switched capacitor and releases the energy as an output stimulus once the voltage reaches a threshold. The control unit utilizes positive feedback to trigger the circuit, so no stimulation control circuit block is needed. An in vivo experiment was performed to demonstrate the performance of the stimulator. Two electromyography (EMG) recording electrodes were implanted into the gastrocnemius muscle of a rat while the ground electrode was attached to the skin.

A free-floating neural implant, which is insensitive to the location, is provided as an inductive link in [10] for wireless energy transmission. The authors have created prototypes of floating implants for precise measurements. The system works with a power transfer efficiency of 2.4% at 60 MHz and provides 1.3 mW power to the implant 14–18 mm away from the transmitter. Their coil link is stable against the lateral and angular misalignments of the floating implants if the coils continue to have the

high-Q resonator. The extra heat produced by the resonator coil also does not exceed safety limits. Recent works of the inductive WPT scheme are evaluated and presented in Table 2. The panel consists of printed and 3D coils. Printed coils maintain acceptable performance under lateral malalignment and are reliable for implants [4].

2.2. Microwave-Based Wireless Power Transfer

Another way to efficiently transmit power wirelessly over long distances in the order of meters to kilometers is microwave power transmission. Figure 4 illustrates the external and implanted antennas' behavior. It should be noted that up-link is defined when the implanted antenna acts as a transmitter and the external antenna act as a receiver, whereas down-link is vice versa.

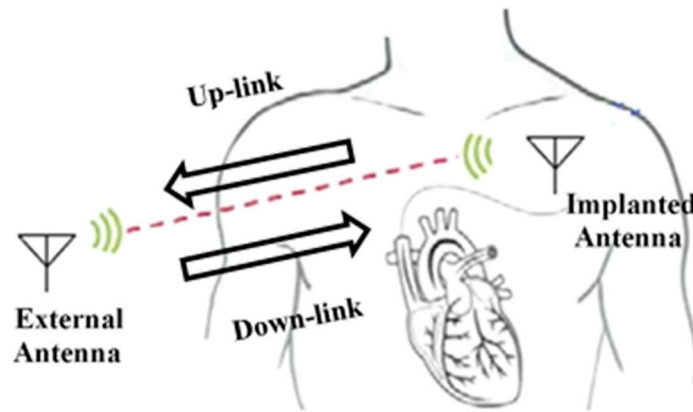


Figure 4. Microwave wireless power transmission (WPT) principle.

Assuming far-field WPT, the budget power link as discussed in [71] can be described as follows:

$$\begin{aligned}
 \text{Link margin (dB/Hz)} &= \left(\frac{C}{N_0}\right)_{\text{Link}} - \left(\frac{C}{N_0}\right)_{\text{Required}} \\
 &= P_{ta} + G_{tg} - L_f + G_{ra} - N_0 - \frac{E_b}{N_0} - 10 \log B_r + G_c - G_d
 \end{aligned}
 \tag{5}$$

where P_{ta} is the transmitted power in dBW, G_{tg} is the transmitting antenna gain in dBi, L_f is the path loss in dB, G_{ra} is the receiving antenna gain in dBi, N_0 is the noise power density in dB/Hz, B_r is the bit rate in kb/s, G_c is the coding gain in dB, and G_d is the fixing deterioration in dB.

The path loss can be calculated through the equation below, taking into consideration that the free-space signal strength reduces with the increase in distance between the transmitter and receiver:

$$L_f = 20 \log\left(\frac{4\pi d}{\lambda}\right)
 \tag{6}$$

where d is the distance between the transmitter and the receiver and λ is the wavelength. Considering the impedance mismatch losses,

$$L_{\text{impedance}} = -10 \log(1 - r^2)
 \tag{7}$$

where r is the appropriate reflection coefficient. Both L_f and $L_{\text{impedance}}$ are considered for more accurate evaluation. The received power by the receiver can be calculated as follows:

$$P_r = P_{ta} + G_{tg} + G_{ra} - L_f - L_{\text{impedance}} - e_p
 \tag{8}$$

where e_p is the polarization mismatch loss between the transmitter and the receiver. Equation (8) can be also described as follows:

$$P_r = \frac{G_{tg}G_{ra}\lambda^2}{(4\pi d)^2}(1 - |S_{11}|^2)(1 - |S_{22}|^2)e_p \times P_t \tag{9}$$

In practice, the received power value for microwave design can be extracted from the value of

$$|S_{21}|^2 = \frac{P_r}{P_t} \tag{10}$$

Table 2. Existing inductive-based WPT approaches for implantable power applications.

Reference	Year	Frequency	Output Power (mW)	Efficiency (%)	Active Range (mm)	Transmitter Dimension (mm)	Receiver Dimension (mm)
[72]	2020	915 MHz	-	1.93	40–50	-	30 × 30
[73]	2020	5.8 GHz	0.01	1.2×10^{-5}	1	-	0.116×0.116
[7]	2019	430 MHz	1000	-	45	-	4.5×3.6
[74]	2019	13.56 MHz	57–447	5.7–44.7	20–50	75 × 75	20 × 30
[34]	2019	434 MHz	31.62	0.68	10	20 × 20	1.6×1.6
[8]	2018	198 MHz	1000	-	140	$d_{outT} = 30.5$	$d_{outR} = 4.9$
[41]	2018	60,300, 330 MHz	-	2.12, 3.88, 1.68	12	$d_{outT} = 17.2, 24, 26$	$d_{outR} = 4$
[75]	2018	2, 4 MHz	126	25	6	$d_{outT} = 35$	$d_{outR} = 20$
[9]	2018	1.3 GHz	3981	-	5	$d_{outT} = 10$	$d_{outR} = 0.2$
[35]	2018	39.86 MHz	115	47.2	-	$d_{outT} = 63.9$	$d_{outR} = 21.56$
[76]	2018	432.5 MHz	1.05	13.9	10	-	-
[77]	2018	430 MHz	-	-	60	30 × 30	10 × 10
[78]	2018	3 MHz	772.8	38.79	5–15	$d_{outT} = 45.2$	$d_{outR} = 36.4$
[11]	2017	13.56 MHz	18	7.7, 11.7	10	$d_{outT} \approx 30$	$d_{outR} = 10$
[40]	2016	50 MHz	0.0657	0.13	10	$d_{outT} = 21$	$d_{outR} = 1$
[19]	2014	8.1 MHz	29.8–93.3	47.6–65.4	12–20	$d_{outT} = 30$	$d_{outR} = 20$
[21]	2019	12.85 MHz	-	75.8	-	30.0×29.6	30.0×29.6
[79]	2019	1–100 MHz	-	-	15	-	$d_{outR} = 1.75$ $d_{inR} = 0.50$
[42]	2018	433 MHz	0.1, 1, 4, 10	0.87	600	-	$d_{outR} = 10$
[29]	2017	13.56 MHz	≤ 100	-	5–15	$d_{outT} = 25$	$d_{outR} = 16$
[10]	2017	60 MHz	1.3	2.4	16	$d_{outT} = 45$	$d_{outR} = 1.2$
[37]	2016	20 MHz	2.2	1.4	10	$d_{outT} = 20, 28$	$d_{outR} = 1$
[43]	2016	40 MHz	-	2.56	70	$d_{outT} = 100$	$d_{outR} = 18$
[30]	2015	2 MHz	1450	27	80	$d_{outT} = 140$	$d_{outR} = 65$
[80]	2015	800 kHz	30 w	95	20	$d_{outT} = 70$	$d_{outR} = 34$
[81]	2012	742 kHz	-	85	0–50	$d_{outT} = 38$	$d_{outR} = 16.5$

It should be noted that some amount of transmitted power will be dissipated in tissue due to radiation and coupling into the body [82]. The implant placement depth plays a key role in the amount of lossy power led by the body tissue. The present-day challenges for this technique include the minimization of energy loss, protecting both humans and animals against exposure to excessive microwave radiation, and the reconfiguring of a wireless transmission system resulting from modifications such as a shifting in range between transmitter and receiver [83]. Microwave WPT can transfer a high amount of power between the transmitter and the receiver circuits. However, it is worth mentioning that human tissues cause problems for the propagation of electromagnetic fields and dilute the electrical field. Therefore, the reflection caused by the lossy mediums reduces the overall power transfer efficiency. Pacemaker implantation is a popular method of curing people with cardiac insufficiency. However, the lifetime of the pacemaker is restricted to the lifespan of the battery and the installation of a subcutaneous pocket [13]. Asif et al. [13] built a rectenna-based leadless pacemaker prototype. For energy transmission to the implanted unit, a wearable transmitting antenna range was fabricated to evaluate the system’s efficiency through Vivo electrocardiogram (ECG) outcomes. The authors assert that the calculations of SAR are within the limits suggested by IEEE and claim that the proposed leadless pacing method is safer, and eliminates the battery, lead, and

device pocket. Zada et al. [84] provided a miniaturized implantable antenna with three frequency bands (902–928, 2400–2483.5, and 1824–1980 MHz) operating at the industrial, scientific, and medical (ISM) band and at the midfield band. A capsule-shaped and a flat type antenna were fabricated with a volume of 647 mm³ and 425.6 mm³, respectively. This triple band antenna was complemented with microelectronics, sensors, and batteries for stimulation in different applications. The system was examined in different tissues, including the scalp, heart, colon, large intestine, and stomach. Asif et al. [85] took advantage of a microwave-based WPT technique to charge deep medical implants like cardiac pacemakers. Their novel wideband numerical model (WBNM) was to provide an RF power source of a leadless pacemaker while using a metamaterial-based antenna operating at 2.4 GHz. They used tissue simulating liquid (TSL) mimicking the human body to prove the performance of their design for implantable applications. A wireless powering technique was introduced by Ho et al. [82], which overcomes the difficulty of miniaturizing the power source via adaptive electromagnetic energy transport. This method is designed for micro-implants like micro-electromechanical system sensors and opto-elements. Figure 5 shows the wireless electrostimulator inserted into the lower epicardium of a rabbit. Recent works of microwave-based WPT systems are reviewed and shown in Table 3.

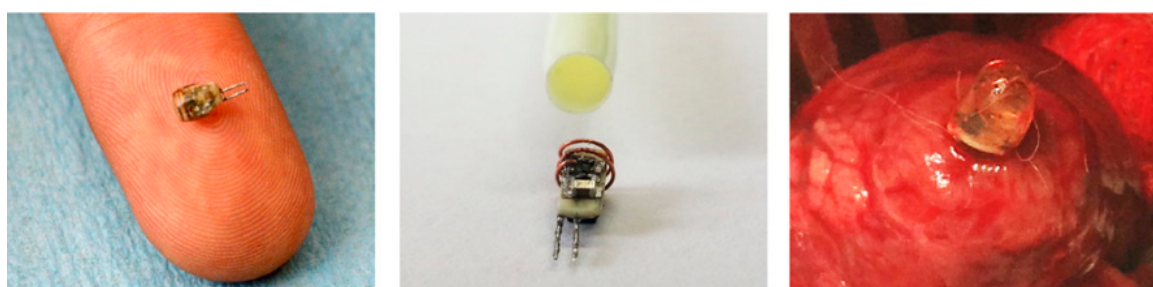


Figure 5. Photograph of the electrostimulator inserted in the lower epicardium of a rabbit via open-chest surgery [82].

Table 3. Existing microwave-based WPT approaches for implantable power applications.

Reference	Year	Frequency	Output Power (mW)	Efficiency (%)	Active Range (mm)	Transmitter Dimensions (mm)	Receiver Dimensions (mm)
[86]	2020	1.47 GHz	6.7	0.67	50	6 × 6	-
[87]	2020	0.403 GHz, 2.44 GHz	-	-	30–350	-	9.5 × 9.5
[88]	2019	1.64 GHz, 3.56 GHz	-	32, 1.1	-	14 × 15	14 × 15
[13]	2019	954 MHz	10	65	110	-	10 × 12
[84]	2018	0.915, 1.9, 2.45 GHz	0.398	-	4.5	-	7 × 6
[38]	2018	400 MHz	19, 82	-	1, 3, 6, 12, 15	d _{outT} = 18	1 × 1
[89]	2018	280 MHz	44	-	3	30 × 80	-
[90]	2017	2.45 GHz	2280, 600, 240, 96	-	1000–4000	-	d _{outR} = 63.6
[91]	2014	2.4 GHz	-	15–78	10–100	63 × 39 × 50	63 × 39 × 50

2.3. Ultrasonic-Based Wireless Power Transfer

The ultrasound imaging is a well-known tool for evaluating patients’ physiological and pathological conditions. In the passive ultrasonic recorder, the backscattered echo is derived from the reaction of biological tissue’s acoustic properties to sound waves. Additionally, the acoustic emission can be used for supplying energy wirelessly in the active biological environment [45]. The ultrasonic-based WPT system has a transmitter converting electrical energy to ultrasonic energy, and a receiver converting back the ultrasonic energy to electrical energy.

The basic model of the implantable ultrasonic coupling WPT system is shown in Figure 6. The transmitting transducer powered by the transmitting module sends the ultrasonic waves, and the ultrasonic energy is transmitted to the receiving transducer through the human tissue. The receiving transducer converts the collected ultrasonic energy into electrical power. Accordingly, power is delivered to the implantable device through the receiving power module. The receiving power processing module mainly includes a voltage-stabilizing circuit and a rectifier circuit.

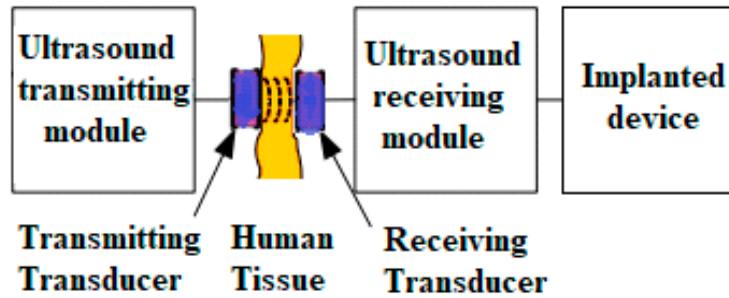


Figure 6. The basic model of the implantable ultrasonic coupling WPT system.

A model of the ultrasonic principle of WPT in the transducer of the transmitter and receiver is shown in Figure 7 [92]; the radiated sound power P is given by the below equation:

$$P = \pi \rho_o c_o u_a^2 a^2 \int_0^a \left[\frac{J_1 \left(ka \frac{1}{\sqrt{l^2 + d^2}} \right)}{l} \right]^2 dl \tag{11}$$

where ρ_o is the density of the medium, c_o is the sound velocity of the medium, u_a is the amplitude, a is the sound source radius of the circular plane A, $k = \frac{\omega}{c_o}$ is the wavenumber of a sound field, d is the distance along the z-axis, and $J_1 \left(ka \frac{1}{\sqrt{l^2 + d^2}} \right)$ is the first-order Bessel function.

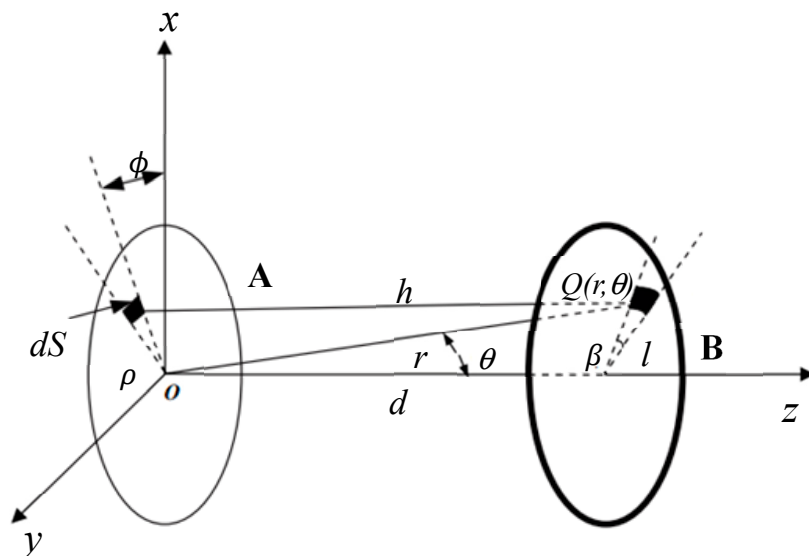


Figure 7. The field model of the ultrasonic coupling wireless transmission system [92].

The ultrasonic-based WPT system is an effective method for medical applications such as cardiac defibrillators and deep brain stimulators (DBSs) [93]. A mode of clinical therapy is a stimulation of excitable tissue for different disorders, such as Parkinson’s disease, urinary incontinence, and heart arrhythmia. The traditional stimulus techniques use percutaneous cables to transport electricity to the electrodes. The classical techniques are dangerous because they can cause infection [12].

The ultrasound- or inductive-based WPT is an interesting solution for this application. The advantage of ultrasound compared to magnetic resonance and induction coupling is that these methods are restricted to a short transfer distance, misalignment issues may occur [94], and the magnetic field intensity must be under specified limitations for the safety of the body exposure. In the ultrasonic method, the operating frequency needs to be changed according to sound radiation and pressure distribution to obtain the optimum energy transition situation [93]. In the range of frequencies individuals hear, Kim et al. [94] have developed an implantable pressure-sensing system driven by mechanical vibration. The pressure inductor has a planar coil with a center of ferrite in which their distance differs from the involved stress. An implantable pressure sensor prototype was designed, as shown in Figure 8, and examined in vitro and in vivo. The acoustic receiver is a piezoelectric cantilever and charges a capacitor by converting sound vibration harmonics into electrical energy. The stored electric charge is discharged across an LC tank with an inductor sensitive to pressure during the period that the cantilever is not shaking.

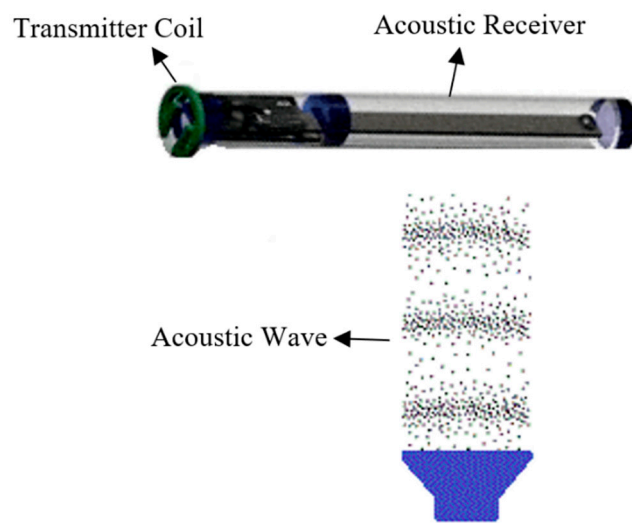


Figure 8. An implantable pressure-sensing system.

Song et al. [95] investigated omnidirectional ultrasonic powering for deep implantable microdevices. When testing the omnidirectionality and outcome of the power transmission under the acoustic Food and Drug Administration (FDA) regulations, the piezoelectric devices with distinct geometries were examined. The receivers were able to produce power in a range of milliwatts with a matched load located 200 mm away from them. The receivers had symmetric geometry of $2 \times 2 \times 2 \text{ mm}^3$ and were insensitive to misalignment. Recent works of ultrasonic-based WPT systems are shown in Table 4.

Table 4. Existing ultrasonic-based WPT approaches for implantable power applications.

Reference	Year	Frequency	Output Power (mW)	Efficiency (%)	Active Range (mm)	Transmitter Dimension (mm)	Receiver Dimension (mm)
[96]	2020	700 kHz	-	-	200	-	$d_{\text{outR}} = 10$
[97]	2017	1 MHz	0.1	-	85	$d_{\text{outT}} = 0.55$	-
[98]	2017	1.8 MHz	-	2.11	30	$d_{\text{outT}} = 10.8, 15.9$	$d_{\text{outR}} = 1.1, 1.2$
[16]	2016	1 MHz	0.184	-	-	-	-
[99]	2016	1 MHz	-	25	3–7	$d_{\text{outT}} = 8$	-
[100]	2015	280 kHz	2.6	18	18	$d_{\text{outT}} = 20$	$d_{\text{outR}} = 20$
[101]	2015	3.4 MHz	0.001	-	100	-	-
[17]	2015	30 MHz	0.1	-	<100	-	$d_{\text{outR}} = 0.7, 1$

Table 4. Cont.

Reference	Year	Frequency	Output Power (mW)	Efficiency (%)	Active Range (mm)	Transmitter Dimension (mm)	Receiver Dimension (mm)
[18]	2014	1 MHz	28	1.6	105	29.6 × 72 *	1 × 5 **
[102]	2013	1.07 MHz	-	45	-	-	-
[103]	2011	1.2 MHz	100	50	-	$d_{outT} = 44$	-
[46]	2011	2.3 MHz	≈0.3	-	30–400	$d_{outT} = 8$	-
[12]	2011	1 MHz	23	-	120	-	$d_{outR} = 8$
[104]	2010	35 kHz	1.23	-	70	-	$d_{outR} = 7$
[105]	2010	673 kHz	1000	27	40	-	-
[106]	2003	100 kHz	5400	36	40	-	-
[25]	2002	1 MHz	2100	20	40	-	-
[26]	2001	1 MHz	-	20	30	-	-

* Width and total length of 48 symmetric elements of the spherical transducer array. ** Active area of a single element of the flat transducer array.

2.4. Hybrid Wireless Power Transfer

A hybrid wireless power transmission (HWPT) system is a combination of two common methods working as a unit system. The inductive WPT system uses magnetic fields to transfer power, whereas the capacitive WPT system uses electric fields. The capacitive WPT approach has two advantages compared with the inductive one. First, there is no eddy current loss and, second, it uses a lightweight and low-cost coupler. However, the capacitive method is limited to small power transfer and short distance because of the small coupling capacitor. When the transfer distance is in several hundred millimeters, the coupling capacitor is usually in the picofarad range. The voltages across the coupling plates of the coupler, which could be improved with double-sided transformers or various compensation topologies (such as double-sided LC and Z-source), are usually hundreds of times the input voltages to enhance the system power level. Considering that the high voltage stressed in the coils of the inductive unit could be fully used as a driving voltage for the capacitive coupler, combining both systems can be done as a hybrid system. Therefore, it is important to take advantage of the inductive and capacitive hybrid system to achieve higher power for HWPT.

A hybrid method includes inductive power transfer and capacitive power transfer, as shown in Figure 9.

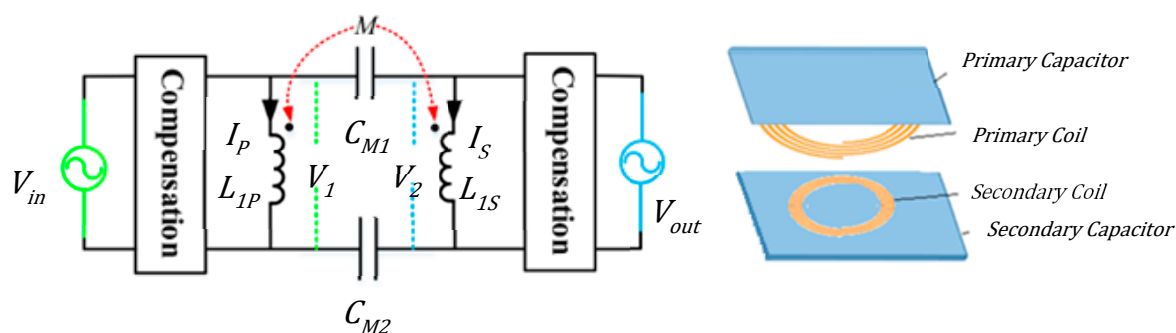


Figure 9. Drawing and diagram of hybrid wireless power transmission (HWPT).

As shown above, the inductive link will generate the alternating magnetic field through coils, which provides the transmission medium. Furthermore, those currents will produce high voltages on the transfer coil because of the self-inductance, whereas the capacitive link system requires high voltages to produce the electric field for the capacitive coupler. Accordingly, the produced voltage on coils of the inductive link system can be used for the capacitive system. A combined system to

construct a hybrid electric power transfer is established in [107]. V_1 and V_2 present the port voltages as follows:

$$V_1 = j\omega L_{1P}I_P + j\omega MI_S \tag{12a}$$

$$V_2 = j\omega L_{1S}I_S + j\omega MI_P \tag{12b}$$

The efficiency of the inductive link is given by the same equation as Equation (4). Whereas the power transfer from the capacitive link of the hybrid system P_{CH} is given by Equation (13):

$$P_{CH} = -\omega^3 CI_P I_S (M^2 - L_{1P}L_{1S}) \tag{13}$$

where I_P and I_S are the RMS currents in primary and secondary coils. L_{1P} and L_{1S} represent the self-inductance of the transmitting and receiving side coils, respectively. M is the mutual inductance.

The advantage of a hybrid system is that it occupies less space than separate units. In this case, there is a capability of having different operating bands, more alternatives, and backup. In [108], the authors proposed a coupled WPT–Power Line Communication (PLC) system that consists of a two-coil resonator system. A four-port system has been designed with two ports dedicated to power transfer and the other two to data transfer. Capacitors have been used to tune the power channel to the desired frequency and improve the matching of the filtering stage to the coupled inductors.

A hybrid inductive-based and a microwave-based WPT system are also presented in [109]. One of the current challenges for wireless transfer for small sensors is to minimize the system size. Haerinia et al. [109] decreased the size of the compact system, at the same time implementing multi-functionality. This goal was obtained by designing an antenna with 14 mm × 15 mm dimensions and having 20 mm × 20 mm dimensions for the hybrid system including the antenna and coil. The coils operating frequency was 510 MHz and the antennas worked at 2.48 GHz and 4.66 GHz. Meng et al. [110] developed a hybrid inductive-ultrasonic WPT link to power biomedical implants over bone, air, and tissue. They optimized cascaded inductive and ultrasonic links for WPT applications. The hybrid link was designed for an air–tissue medium to operate at 1.1 MHz with a power transmission efficiency of 0.16%. Recent works related to the HWPT system are shown in Table 5. The receiver dimension should be as small as possible to make it more convenient for implant applications. In case the receiver dimension is larger than 40 mm, such design can be printed on a flexible material substrate such as Kapton to facilitate the surgery procedures [111]. It is worth mentioning that rotational/lateral misalignment and bending are two conditions that may happen because of changes in the implanted antenna location or the person’s movement. Therefore, the bending of a flexible substrate and the misalignment effect must be investigated precisely [112].

Table 5. Existing HWPT approaches for implantable power applications.

Reference	Year	Frequency	Output Power (mW)	Efficiency (%)	Active Range (mm)	Transmitter Dimension (mm)	Receiver Dimension (mm)	Methods
[109]	2019	510 MHz, 2.48 GHz, 4.66 GHz	0.0004	3.7, 2.2, 1	20–60	$d_{outT} = 39.75$	$d_{outR} = 20$	Inductive and Microwave
[113]	2018	4 MHz	500, 53, 53	1.9, 2.6, 0.98	>30,15,30	-	$d_{outR} = 40,83,83$	Inductive and Capacitive
[114]	2020	13.56 MHz, 415 MHz, 905 MHz, 1300 MHz	-	10, 0.5, 4.6, 6.5	15–110	$d_{outT} = 79.6$	$d_{outR} = 31.5$	Inductive and Microwave
[115]	2017	13.56 MHz/910 MHz	-	17	16	$d_{outT} = 83.2$	$d_{outR} = 24.2$	Inductive and Microwave
[110]	2017	1.1 MHz	-	0.16	60	$d_{outT} = 100$	$d_{outR} = 15$	Inductive and Ultrasonic
[116]	2012	200 kHz	8	1	70	$d_{outT} = 39$	$d_{outR} = 33$	Inductive and Ultrasonic

3. Consideration for Design of Medical implants and Related Regulations

Developments in wireless technology for medical devices are elevating the provision of healthcare with lower expenses. Wireless telecommunications can be used for both wearable and implantable applications, such as DBSs, tracking of vital signs, measuring biological parameters, and cardiac rhythm control. The main advantage of wireless technology compared to landline networks is that the patient is not required to be linked to a certain location by cables [117]. Despite advances in biomedical implants such as the pacemaker, cochlear implant, and nerve stimulator, these devices need to be improved in terms of miniaturization, the biocompatibility of materials, sources of electric charge, and wireless communication. To develop an effective IMD, the doctor, the patient, and the technician must collaborate in collecting coherent initial information about different aspects of the device. In particular, the user's satisfaction, the doctor's technical priorities, and the workability of the model are necessary to be considered in the design process [118]. There are important factors for designing medical implants. Since an electric device is implanted inside the human body, the organisms around the device may react to it. To avoid such an issue, the device should be made up of or coated by biocompatible materials. Moreover, the medical implants should have appropriate packaging to isolate components of the device from body tissue.

Another factor is the structure of the design itself. Before the design, enough data should be collected from patients, engineers, and previous designs, along with their advantages and drawbacks [118]. The United States' medical devices market is regulated by three different organizations: the Federal Communications Commission (FCC), the Food and Drug Administration (FDA), and the Centers for Medicare and Medicaid Services (CMS). Wireless medical instruments can be classified into two categories: short-range, such as inductive implants and medical body area networks, and long-range, such as wireless medical telemetry (WMTS). According to the FCC, short-range technology sends data to local receivers and long-range technology sends user data to a remote spot [117]. The FDA's mission is to check if the proposed medical devices guarantee the factors of safeness and effectiveness for patient usage. The FDA divides medical devices into three classifications based on the risk factor. Class I includes the lowest-risk devices, and without FDA prior authorization, medical devices in this class may be advertised. The medical devices using wireless technologies are usually considered in Class II. The highest-risk medical devices fall under Class III and clinical trials are mandatory to get FDA approval. The FCC and FDA must permit before wireless medical devices can be marketed in the United States. It is worth mentioning that the FDA and FCC have distinct criteria, and one agency's authorization does not simply ensure the other's consent [117].

The designers of medical implants are currently dealing with challenges in materials, output power, size miniaturization, the efficiency of the wireless link, and cybersecurity [118]. There are different types of cyber-attacks, including theft of protected health information and execution of fraudulent device commands, which require appropriate cybersecurity mechanisms [119]. It is crucial to have a broad perspective of different aspects of wireless techniques before choosing the tactic for any specific applications. Figure 10 shows a comparison between the collected research papers for different approaches: the maximum dimension of a receiver, power transfer efficiency, and frequency.

From Figure 10a,b, it can be seen that most of the ultrasound-based WPT systems work at a low operating frequency, ranging from a few hundred kHz up to few MHz. Most likely, inductive-based WPT systems mostly operate at a low operating frequency but range at a higher frequency compared to ultrasound-based and reach up to a few hundred MHz. Moreover, it can be concluded that operating frequency for most of the research based on inductive WPT lay below 50 MHz. Furthermore, 13.56 MHz is the interest frequency for the majority of the inductive WPT research field. On the contrary, most of the collected papers' research related to microwave-based WPT located at a higher operating frequency; compared to both ultrasound-based and inductive-based WPT, it ranged from hundreds of MHz to hundreds of GHz. On the other hand, it was noticed that the operating frequency of hybrid wireless power transmission (HWPT) varies from low to high frequency. This is due to the fact that HWPT

comprises a combination of more than one method to transfer power wirelessly, such as inductive-based and capacitive-based.

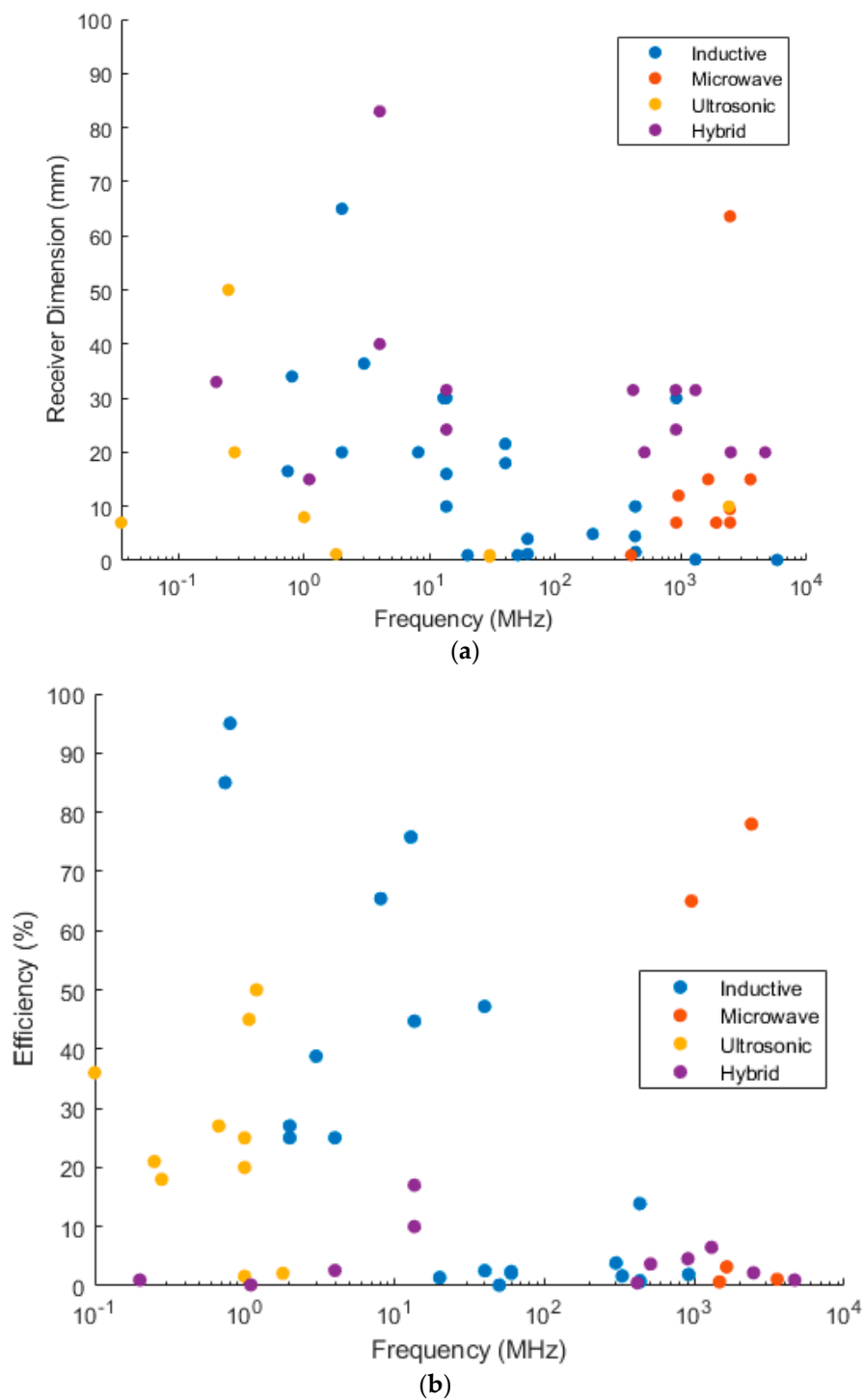


Figure 10. A comparison of different approaches. (a) Maximum dimension of receiver versus frequency; (b) Efficiency versus frequency.

Figure 10a presents the maximum dimensions of the receiver versus the operating frequency. In general, it can be noticed that most of the receivers' dimensions are less than 30 mm for all the WPT-based methods. This is due to the fact that miniaturization of the implanted device is highly recommended in the medical field to simplify the surgery procedures and to be more comfortable for

the patients. Besides, it is shown in Figure 10a that the receiver dimensions of HWPT have a larger size compared to the other methods of WPT. Moreover, the receiver dimensions for most of the collected research on ultrasound-based and microwave-based WPT are below 20 mm. Additionally, a cluster of biomedical implant receivers using the inductive-based technique have a maximum dimension of less than 20 mm and operate at a considerably lower frequency compared to the microwave-based technique with almost the same size.

Figure 10b presents the efficiency percentage versus the operating frequency. In general, it can be interpreted that the maximum power transmission efficiency is achieved via inductive-based WPT, whereas the minimum power transmission efficiency is achieved via HWPT; on the other hand, the maximum efficiencies achieved are 78% and 50% for microwave-based and ultrasound-based WPT, respectively. In the same way, we conclude from Figure 10b that the operating frequency is much higher for microwave-based WPT compared to inductive-based WPT, which has almost the same efficiency.

4. Conclusions

This research has evaluated and discussed a survey of the following popular methods for wirelessly transferring power into IMDs: (1) inductive-based WPT, (2) microwave-based WPT, (3) ultrasound-based WPT, and (4) hybrid wireless power transmission (HWPT). In this research, the power delivered in the reviewed works to medical implants varied from a few μW to 5.4 W, with distance ranges from 1 mm to 4 m and maximum efficiency of up to 95%. Based on collected papers' research, it was concluded that ultrasound-based and inductive-based WPT works at low operating frequency (less than 50 MHz), whereas the microwave-based WPT typically works at a higher frequency. On the other hand, the HWPT could be found at a low or high operating frequency, depending on the combination used. It can be seen that the receiver dimension was less than 30 mm for all the WPT-based methods. Furthermore, HWPT had a bigger receiver size. The maximum power transfer efficiency was conducted via inductive-based WPT. Based on collected papers, the value of achievable maximum efficiencies were 95%, 78%, 50%, and 17% for inductive-based, microwave-based, ultrasound-based, and HWPT, respectively. This paper provides a perspective on different WPT approaches for biomedical applications by investigating the significant works in this field. Additionally, some points for designing effective IMDs and related commercial rules and regulations are presented.

Author Contributions: Conceptualization, M.H. and R.S.; methodology, M.H. and R.S.; investigation, M.H. and R.S.; resources, M.H.; writing—original draft preparation, M.H.; writing—review and editing, M.H. and R.S.; visualization, M.H. and R.S.; supervision, M.H.; project administration, M.H. All authors have read and agreed to the published version of the manuscript.

Funding: The financial support of the School of Electrical Engineering and Computer Science, University of North Dakota, is acknowledged.

Conflicts of Interest: The authors declare no conflict of interest.

References

1. Ben Amar, A.; Kouki, A.B.; Cao, H. Power Approaches for Implantable Medical Devices. *Sensors* **2015**, *15*, 28889–28914. [[CrossRef](#)] [[PubMed](#)]
2. Taalla, R.V.; Arefin, S.; Kaynak, A.; Kouzani, A. A Review on Miniaturized Ultrasonic Wireless Power Transfer to Implantable Medical Devices. *IEEE Access* **2018**, *7*, 2092–2106. [[CrossRef](#)]
3. Shadid, R.; Noghianian, S. A Literature Survey on Wireless Power Transfer for Biomedical Devices. *Int. J. Antennas Propag.* **2018**, *2018*, 1–11. [[CrossRef](#)]
4. Mutashar, S.; Hannan, M.A.; Samad, S.A.; Hussain, A. Analysis and Optimization of Spiral Circular Inductive Coupling Link for Bio-Implanted Applications on Air and within Human Tissue. *Sensors* **2014**, *14*, 11522–11541. [[CrossRef](#)]

5. Yu, Y.; Hao, H.; Wang, W.; Li, L. Simulative and experimental research on wireless power transmission technique in implantable medical device. *IEEE Annu. Int. Conf. Eng. Med. Biol. Soc.* **2009**, 923–926. [[CrossRef](#)]
6. Bocan, K.N.; Sejdić, E. Adaptive Transcutaneous Power Transfer to Implantable Devices: A State of the Art Review. *Sensors* **2016**, *16*, 393. [[CrossRef](#)] [[PubMed](#)]
7. Lyu, H.; Gad, P.; Zhong, H.; Edgerton, V.R.; Babakhani, A. A 430-MHz wirelessly powered implantable pulse generator with intensity/rate control and sub-1 μ A quiescent current consumption. *IEEE Trans. Biomed. Circuits Syst.* **2018**, *13*, 180–190.
8. Lyu, H.; Wang, J.; La, J.-H.; Chung, J.M.; Babakhani, A. An Energy-Efficient Wirelessly Powered Millimeter-Scale Neurostimulator Implant Based on Systematic Codesign of an Inductive Loop Antenna and a Custom Rectifier. *IEEE Trans. Biomed. Circuits Syst.* **2018**, *12*, 1131–1143. [[CrossRef](#)]
9. Khalifa, A.; Karimi, Y.; Wang, Q.; Garikapati, S.; Montlouis, W.; Stanacevic, M.; Thakor, N.; Etienne-Cummings, R. The Microbead: A Highly Miniaturized Wirelessly Powered Implantable Neural Stimulating System. *IEEE Trans. Biomed. Circuits Syst.* **2018**, *12*, 521–531. [[CrossRef](#)]
10. Mirbozorgi, S.A.; Yeon, P.; Ghovanloo, M. Robust Wireless Power Transmission to mm-Sized Free-Floating Distributed Implants. *IEEE Trans. Biomed. Circuits Syst.* **2017**, *11*, 692–702. [[CrossRef](#)]
11. Yang, C.-L.; Chang, C.-K.; Lee, S.-Y.; Chang, S.-J.; Chiou, L.-Y. Efficient Four-Coil Wireless Power Transfer for Deep Brain Stimulation. *IEEE Trans. Microw. Theory Tech.* **2017**, *65*, 2496–2507. [[CrossRef](#)]
12. Larson, P.J.; Towe, B.C. Miniature ultrasonically powered wireless nerve cuff stimulator. In Proceedings of the 2011 5th International IEEE/EMBS Conference on Neural Engineering, Cancun, Mexico, 27 April–1 May 2011; pp. 265–268.
13. Asif, S.M.; Iftikhar, A.; Hansen, J.W.; Khan, M.S.; Ewert, D.L.; Braaten, B.D. A Novel RF-Powered Wireless Pacing via a Rectenna-Based Pacemaker and a Wearable Transmit-Antenna Array. *IEEE Access* **2019**, *7*, 1139–1148. [[CrossRef](#)]
14. Zargham, M.; Gulak, P.G. A 0.13 μ m CMOS integrated wireless power receiver for biomedical applications. In Proceedings of the 2013 ESSCIRC (ESSCIRC), Bucharest, Romania, 16–20 September 2013; pp. 137–140.
15. Keikhosrav, K.; Kamalinejad, P.; Mirabbasi, S.; Takahata, K.; Leung, V.C. An ultra-low-power monitoring system for inductively coupled biomedical implants. In Proceedings of the 2013 IEEE International Symposium on Circuits and Systems (ISCAS2013), Beijing, China, 19–23 May 2013.
16. Mazzilli, F.; Dehollain, C. 184 μ W ultrasonic on-off keying/amplitude-shift keying demodulator for downlink communication in deep implanted medical devices. *Electron. Lett.* **2016**, *52*, 502–504. [[CrossRef](#)]
17. Charthad, J.; Weber, M.J.; Chang, T.C.; Arbabian, A. A mm-Sized Implantable Medical Device (IMD) with Ultrasonic Power Transfer and a Hybrid Bi-Directional Data Link. *IEEE J. Solid State Circuits* **2015**, *50*, 1741–1753. [[CrossRef](#)]
18. Mazzilli, F.; Lafon, C.; Dehollain, C. A 10.5 cm Ultrasound Link for Deep Implanted Medical Devices. *IEEE Trans. Biomed. Circuits Syst.* **2014**, *8*, 738–750. [[CrossRef](#)] [[PubMed](#)]
19. Ahn, D.; Hong, S. Wireless Power Transmission with Self-Regulated Output Voltage for Biomedical Implant. *IEEE Trans. Ind. Electron.* **2013**, *61*, 2225–2235. [[CrossRef](#)]
20. Kilinc, E.G.; Ghanad, M.A.; Maloberti, F.; Dehollain, C. Short range remote powering of implanted electronics for freely moving animals. In Proceedings of the 2013 IEEE 11th International New Circuits and Systems Conference (NEWCAS), Paris, France, 16–19 June 2013.
21. Lyu, H.; Jian, Z.; Liu, X.; Sun, Y.; Babakhani, A. Towards the Implementation of a Wirelessly Powered Dielectric Sensor with Digitized Output for Implantable Applications. *IEEE Sensors Lett.* **2019**, *3*, 1–4. [[CrossRef](#)]
22. Kilinc, E.G.; Dehollain, C.; Maloberti, F. A low-power PPM demodulator for remotely powered batteryless implantable devices. In Proceedings of the 2014 IEEE 57th International Midwest Symposium on Circuits and Systems (MWSCAS), College Station, TX, USA, 3–6 August 2014.
23. Zargham, M.; Gulak, P.G. Fully integrated on-chip coil in 0.13 μ m CMOS for wireless power transfer through biological media. *IEEE Trans. Biomed. Circuits Syst.* **2015**, *9*, 259–271. [[CrossRef](#)]
24. Adeeb, M.A.; Islam, A.B.; Haider, M.R.; Tulip, F.S.; Ericson, M.N.; Islam, S.K. An Inductive Link-Based Wireless Power Transfer System for Biomedical Applications. *Act. Passiv. Electron. Compon.* **2012**, *2012*, 1–11. [[CrossRef](#)]

25. Suzuki, S.-N.; Kimura, S.; Katane, T.; Saotome, H.; Saito, O.; Kobayashi, K. Power and Interactive Information Transmission to Implanted Medical Device Using Ultrasonic. *Jpn. J. Appl. Phys.* **2002**, *41*, 3600–3603. [[CrossRef](#)]
26. Kawanabe, H.; Katane, T.; Saotome, H.; Saito, O.; Kobayashi, K. Power and Information Transmission to Implanted Medical Device Using Ultrasonic. *Jpn. J. Appl. Phys.* **2001**, *40*, 3865–3866. [[CrossRef](#)]
27. Kilinc, E.G.; Moya, A.C.; Van Lintel, H.; Renaud, P.; Maloberti, F.; Wang, Q.; Dehollain, C.; Renaud, P. Remotely powered implantable heart monitoring system for freely moving animals. In Proceedings of the 5th IEEE International Workshop on Advances in Sensors and Interfaces IWASI, Bari, Italy, 13–14 June 2013.
28. Simard, G.; Sawan, M.; Massicotte, D. High-Speed OQPSK and Efficient Power Transfer Through Inductive Link for Biomedical Implants. *IEEE Trans. Biomed. Circuits Syst.* **2010**, *4*, 192–200. [[CrossRef](#)] [[PubMed](#)]
29. Jiang, D.; Cirmirakis, D.; Schormans, M.; Perkins, T.A.; Donaldson, N.; Demosthenous, A. An Integrated Passive Phase-Shift Keying Modulator for Biomedical Implants with Power Telemetry Over a Single Inductive Link. *IEEE Trans. Biomed. Circuits Syst.* **2016**, *11*, 64–77. [[CrossRef](#)] [[PubMed](#)]
30. Kiani, M.; Lee, B.; Yeon, P.; Ghovanloo, M. A Q-Modulation Technique for Efficient Inductive Power Transmission. *IEEE J. Solid State Circuits* **2015**, *50*, 2839–2848. [[CrossRef](#)]
31. Lu, Z.; Sawan, M. An 8 Mbps data rate transmission by inductive link dedicated to implantable devices. In Proceedings of the 2008 IEEE International Symposium on Circuits and Systems, Seattle, WA, USA, 18–21 May 2008.
32. Mandal, S.; Sarpeshkar, R. Power-efficient impedance-modulation wireless data links for biomedical implants. *IEEE Trans. Biomed. Circuits Syst.* **2008**, *2*, 301–315. [[CrossRef](#)]
33. Brizi, D.; Fontana, N.; Barmada, S.; Monorchio, A. A Multi-Transmitter Configuration for High-Safety Wireless Power Transfer Applications. In Proceedings of the 2019 International Applied Computational Electromagnetics Society Symposium (ACES), Miami, FL, USA, 14–19 April 2019; pp. 1–2.
34. Rahmani, H.; Babakhani, A. A Dual-Mode RF Power Harvesting System with an On-Chip Coil in 180-nm SOI CMOS for Millimeter-Sized Biomedical Implants. *IEEE Trans. Microw. Theory Tech.* **2019**, *67*, 414–428. [[CrossRef](#)]
35. Sun, G.; Muneer, B.; Li, Y.; Zhu, Q. Ultracompact Implantable Design with Integrated Wireless Power Transfer and RF Transmission Capabilities. *IEEE Trans. Biomed. Circuits Syst.* **2018**, *12*, 281–291. [[CrossRef](#)]
36. Institute of Electrical and Electronics Engineers. *IEEE Standard for Safety Levels with Respect to Human Exposure to Radio Frequency Electromagnetic Fields, 3 kHz to 300 GHz*; IEEE: Piscataway, NJ, USA, 1999; ISBN 155937179X.
37. Ibrahim, A.; Kiani, M. A Figure-of-Merit for Design and Optimization of Inductive Power Transmission Links for Millimeter-Sized Biomedical Implants. *IEEE Trans. Biomed. Circuits Syst.* **2016**, *10*, 1100–1111. [[CrossRef](#)]
38. Manoufali, M.; Bialkowski, K.; Mohammed, B.J.; Abbosh, A.M. Wireless Power Link Based on Inductive Coupling for Brain Implantable Medical Devices. *IEEE Antennas Wirel. Propag. Lett.* **2017**, *17*, 160–163. [[CrossRef](#)]
39. Chen, P.; Yang, H.; Luo, R.; Zhao, B. A Tissue-Channel Transcutaneous Power Transfer Technique for Implantable Devices. *IEEE Trans. Power Electron.* **2018**, *33*, 9753–9761. [[CrossRef](#)]
40. Ibrahim, A.; Kiani, M. Inductive power transmission to millimeter-sized biomedical implants using printed spiral coils. In Proceedings of the 2016 38th Annual International Conference of the IEEE Engineering in Medicine and Biology Society (EMBC), Orlando, FL, USA, 16–20 August 2016.
41. Feng, P.; Yeon, P.; Cheng, Y.; Ghovanloo, M.; Constandinou, T.G. Chip-Scale Coils for Millimeter-Sized Bio-Implants. *IEEE Trans. Biomed. Circuits Syst.* **2018**, *12*, 1088–1099. [[CrossRef](#)] [[PubMed](#)]
42. Faerber, J.; Gregson, R.; Clutton, R.E.; Khan, S.R.; Cochran, S.; Desmulliez, M.P.Y.; Cummins, G.; Pavuluri, S.K.; Record, P.; Rodriguez, A.R.A.; et al. In Vivo Characterization of a Wireless Telemetry Module for a Capsule Endoscopy System Utilizing a Conformal Antenna. *IEEE Trans. Biomed. Circuits Syst.* **2017**, *12*, 95–105. [[CrossRef](#)] [[PubMed](#)]
43. Gougheri, H.S.; Kiani, M. Optimal frequency for powering millimeter-sized biomedical implants inside an inductively-powered homecage. In Proceedings of the 2016 38th Annual International Conference of the IEEE Engineering in Medicine and Biology Society (EMBC), Orlando, FL, USA, 16–20 August 2016.
44. Silay, K.M.; Dehollain, C.; Declercq, M. A Closed-Loop Remote Powering Link for Wireless Cortical Implants. *IEEE Sens. J.* **2013**, *13*, 3226–3235. [[CrossRef](#)]

45. Rosa, B.M.G.; Yang, G.Z. Active implantable sensor powered by ultrasounds with application in the monitoring of physiological parameters for soft tissues. In Proceedings of the 2016 IEEE 13th International Conference on Wearable and Implantable Body Sensor Networks (BSN), San Francisco, CA, USA, 14–17 June 2016.
46. Maleki, T.; Cao, N.; Song, S.H.; Kao, C.; Ko, S.-C.A.; Ziaie, B. An Ultrasonically Powered Implantable Micro-Oxygen Generator (IMOG). *IEEE Trans. Biomed. Eng.* **2011**, *58*, 3104–3111. [[CrossRef](#)] [[PubMed](#)]
47. Shadid, R.; Haerinia, M.; Noghanian, S. Study of Rotation and Bending Effects on a Flexible Hybrid Implanted Power Transfer and Wireless Antenna System. *Sensors* **2020**, *20*, 1368. [[CrossRef](#)] [[PubMed](#)]
48. Bocan, K.N.; Mickle, M.H.; Sejdić, E. Multi-Disciplinary Challenges in Tissue Modeling for Wireless Electromagnetic Powering: A Review. *IEEE Sens. J.* **2017**, *17*, 6498–6509. [[CrossRef](#)]
49. Yang, C.-H.; Li, W.; Chen, R.K.-R. Determination of Tissue Thermal Conductivity as a Function of Thermal Dose and Its Application in Finite Element Modeling of Electrosurgical Vessel Sealing. *IEEE Trans. Biomed. Eng.* **2020**, *67*, 2862–2869. [[CrossRef](#)] [[PubMed](#)]
50. Hao, J.-J.; Lv, L.-J.; Ju, L.; Xie, X.; Liu, Y.-J.; Yang, H. Simulation of microwave propagation properties in human abdominal tissues on wireless capsule endoscopy by FDTD. *Biomed. Signal Process. Control.* **2019**, *49*, 388–395. [[CrossRef](#)]
51. Fornes-Leal, A.; Cardona, N.; Frasson, M.; Castello-Palacios, S.; Nevarez, A.; Beltran, V.P.; Garcia-Pardo, C. Dielectric Characterization of In Vivo Abdominal and Thoracic Tissues in the 0.5–26.5 GHz Frequency Band for Wireless Body Area Networks. *IEEE Access* **2019**, *7*, 31854–31864. [[CrossRef](#)]
52. Braun, J.; Tzschätzsch, H.; Körting, C.; De Schellenberger, A.A.; Jenderka, M.; Drießle, T.; Ledwig, M.; Sack, I. A compact 0.5 T MR elastography device and its application for studying viscoelasticity changes in biological tissues during progressive formalin fixation. *Magn. Reson. Med.* **2017**, *79*, 470–478. [[CrossRef](#)]
53. Bocan, K.N.; Mickle, M.H.; Sejdić, E. Simulating, Modeling, and Sensing Variable Tissues for Wireless Implantable Medical Devices. *IEEE Trans. Microw. Theory Tech.* **2018**, *66*, 3547–3556. [[CrossRef](#)]
54. Gun, L.; Ning, D.; Liang, Z. Effective Permittivity of Biological Tissue: Comparison of Theoretical Model and Experiment. *Math. Probl. Eng.* **2017**, *2017*, 1–7. [[CrossRef](#)]
55. Balidemaj, E.; De Boer, P.; Van Lier, A.L.H.M.W.; Remis, R.F.; Stalpers, L.J.A.; Westerveld, G.H.; Nederveen, A.J.; Berg, C.A.T.V.D.; Crezee, J. In vivo electric conductivity of cervical cancer patients based on B+1 maps at 3T MRI. *Phys. Med. Biol.* **2016**, *61*, 1596–1607. [[CrossRef](#)] [[PubMed](#)]
56. Dahdouh, S.; Varsier, N.; Ochoa, M.A.N.; Wiart, J.; Peyman, A.; Bloch, I. Infants and young children modeling method for numerical dosimetry studies: Application to plane wave exposure. *Phys. Med. Biol.* **2016**, *61*, 1500–1514. [[CrossRef](#)] [[PubMed](#)]
57. Mobashsher, A.T.; Mahmoud, A.; Abbosh, A.M. Portable Wideband Microwave Imaging System for Intracranial Hemorrhage Detection Using Improved Back-projection Algorithm with Model of Effective Head Permittivity. *Sci. Rep.* **2016**, *6*, 20459. [[CrossRef](#)]
58. Jilani, M.T.; Wen, W.P.; Cheong, L.Y.; Rehman, M.Z.U. A Microwave Ring-Resonator Sensor for Non-Invasive Assessment of Meat Aging. *Sensors* **2016**, *16*, 52. [[CrossRef](#)]
59. Diao, Y.; Leung, S.-W.; Chan, K.H.; Sun, W.; Siu, Y.-M.; Kong, R. The effect of gaze angle on the evaluations of sar and temperature rise in human eye under plane-wave exposures from 0.9 to 10 ghz. *Radiat. Prot. Dosim.* **2015**, *172*, 393–400. [[CrossRef](#)]
60. Abdelaziz, A.F.; Abbasi, Q.H.; Yang, K.; Qaraqe, K.; Hao, Y.; Alomainy, A. Terahertz signal propagation analysis inside the human skin. In Proceedings of the 2015 IEEE 11th International Conference on Wireless and Mobile Computing, Networking and Communications (WiMob), Abu Dhabi, UAE, 19–21 October 2015; pp. 15–19.
61. Li, C.; Chen, Q.; Xie, Y.; Wu, T. Dosimetric study on eye's exposure to wide band radio frequency electromagnetic fields: Variability by the ocular axial length. *Bioelectromagnetics* **2014**, *35*, 324–336. [[CrossRef](#)]
62. Zhang, X.; Zhu, S.; He, B. Imaging electric properties of biological tissues by RF field mapping in MRI. *IEEE Trans. Med. Imaging* **2010**, *29*, 474–481. [[CrossRef](#)]
63. Peyman, A.; Gabriel, C.; Grant, E.H.; Vermeeren, G.; Martens, L. Variation of the dielectric properties of tissues with age: The effect on the values of SAR in children when exposed to walkie-talkie devices. *Phys. Med. Biol.* **2009**, *54*, 227–241. [[CrossRef](#)]

64. Keshvari, J.; Keshvari, R.; Lang, S. The effect of increase in dielectric values on specific absorption rate (SAR) in eye and head tissues following 900, 1800 and 2450 MHz radio frequency (RF) exposure. *Phys. Med. Biol.* **2006**, *51*, 1463–1477. [[CrossRef](#)] [[PubMed](#)]
65. Ryckaert, J.; De Doncker, P.; Meys, R.; De Le Hoye, A.; Donnay, S. Channel model for wireless communication around human body. *Electron. Lett.* **2004**, *40*, 543. [[CrossRef](#)]
66. Nagaoka, T.; Watanabe, S.; Sakurai, K.; Kunieda, E.; Watanabe, S.; Taki, M.; Yamanaka, Y. Development of realistic high-resolution whole-body voxel models of Japanese adult males and females of average height and weight, and application of models to radio-frequency electromagnetic-field dosimetry. *Phys. Med. Biol.* **2003**, *49*, 1–15. [[CrossRef](#)] [[PubMed](#)]
67. Monebhurrun, V.; Dale, C.; Bolomey, J.-C.; Wiart, J. A numerical approach for the determination of the tissue equivalent liquid used during SAR assessments. *IEEE Trans. Magn.* **2002**, *38*, 745–748. [[CrossRef](#)]
68. Sun, T.; Xie, X.; Wang, Z. *Wireless Power Transfer for Medical Microsystems*; Springer: New York, NY, USA, 2013; p. 183.
69. Ali, H.; Ahmad, T.J.; Khan, S.A. Inductive link design for medical implants. In Proceedings of the 2009 IEEE Symposium on Industrial Electronics & Applications, Kuala Lumpur, Malaysia, 4–6 October 2009.
70. Low, Z.N.; Chinga, R.A.; Tseng, R.; Lin, J. Design and Test of a High-Power High-Efficiency Loosely Coupled Planar Wireless Power Transfer System. *IEEE Trans. Ind. Electron.* **2008**, *56*, 1801–1812. [[CrossRef](#)]
71. Xia, W.; Saito, K.; Takahashi, M.; Ito, K. Performances of an Implanted Cavity Slot Antenna Embedded in the Human Arm. *IEEE Trans. Antennas Propag.* **2009**, *57*, 894–899. [[CrossRef](#)]
72. Zhang, K.; Liu, C.; Jiang, Z.; Zhang, Y.; Liu, X.; Guo, H.; Yang, X. Near-Field Wireless Power Transfer to Deep-Tissue Implants for Biomedical Applications. *IEEE Trans. Antennas Propag.* **2019**, *68*, 1098–1106. [[CrossRef](#)]
73. Zhao, B.; Kuo, N.-C.; Liu, B.; Li, Y.-A.; Iotti, L.; Niknejad, A.M. A Batteryless Padless Crystalless $116\mu \times 116\mu\text{m}$ “Dielet” Near-Field Radio with On-Chip Coil Antenna. *IEEE J. Solid State Circuits* **2019**, *55*, 249–260. [[CrossRef](#)]
74. Javan-Khoshkholgh, A.; Sassoon, J.C.; Farajidavar, A. A Wireless Rechargeable Implantable System for Monitoring and Pacing the Gut in Small Animals. In Proceedings of the 2019 IEEE Biomedical Circuits and Systems Conference (BioCAS), Nara, Japan, 17–19 October 2019; pp. 1–4. [[CrossRef](#)]
75. Ahmadi, M.M.; Ghandi, S. A Class-E Power Amplifier with Wideband FSK Modulation for Inductive Power and Data Transmission to Medical Implants. *IEEE Sens. J.* **2018**, *18*, 7242–7252. [[CrossRef](#)]
76. Quadir, N.A.; Albasha, L.; Taghadosi, M.; Qaddoumi, N.; Hatahet, B. Low-Power Implanted Sensor for Orthodontic Bond Failure Diagnosis and Detection. *IEEE Sens. J.* **2018**, *18*, 3003–3009. [[CrossRef](#)]
77. Li, L.; Liu, H.; Zhang, H.; Xue, W. Efficient Wireless Power Transfer System Integrating with Metasurface for Biological Applications. *IEEE Trans. Ind. Electron.* **2017**, *65*, 3230–3239. [[CrossRef](#)]
78. Haerinia, M. Modeling and simulation of inductive-based wireless power transmission systems. In *Book Energy Harvesting for Wireless Sensor Networks: Technology, Components and System Design*, 1st ed.; Olfa, K., Ed.; De Gruyter: Berlin, Germany; Boston, MA, USA, 2018; pp. 197–220.
79. Cheng, Y.; Chen, G.; Xuan, D.; Qian, G.; Ghovanloo, M.; Wang, G. Analytical Modeling of Small, Solenoidal, and Implantable Coils with Ferrite Tube Core. *IEEE Microw. Wirel. Compon. Lett.* **2019**, *29*, 237–239. [[CrossRef](#)]
80. Knecht, O.; Bosshard, R.; Kolar, J.W. High-Efficiency Transcutaneous Energy Transfer for Implantable Mechanical Heart Support Systems. *IEEE Trans. Power Electron.* **2015**, *30*, 6221–6236. [[CrossRef](#)]
81. Li, X.; Zhang, H.; Peng, F.; Li, Y.; Yang, T.; Wang, B.; Fang, D. A Wireless Magnetic Resonance Energy Transfer System for Micro Implantable Medical Sensors. *Sensors* **2012**, *12*, 10292–10308. [[CrossRef](#)] [[PubMed](#)]
82. Ho, J.S.; Yeh, A.J.; Neofytou, E.; Kim, S.; Tanabe, Y.; Patlolla, B.; Beygui, R.E.; Poon, A.S.Y. Wireless power transfer to deep-tissue microimplants. *Proc. Natl. Acad. Sci. USA* **2014**, *111*, 7974–7979. [[CrossRef](#)] [[PubMed](#)]
83. Lu, M. Microwave Power Transmission Based on Retro-reflective Beamforming. In *Wireless Power Transfer—Fundamentals and Technologies*; Coca, E., Ed.; In Tech: London, UK, 2016.
84. Zada, M.; Yoo, H. A Miniaturized Triple-Band Implantable Antenna System for Bio-Telemetry Applications. *IEEE Trans. Antennas Propag.* **2018**, *66*, 7378–7382. [[CrossRef](#)]
85. Asif, S.M.; Iftikhar, A.; Braaten, B.D.; Ewert, D.L.; Maile, K. A Wide-Band Tissue Numerical Model for Deeply Implantable Antennas for RF-Powered Leadless Pacemakers. *IEEE Access* **2019**, *7*, 31031–31042. [[CrossRef](#)]

86. Basir, A.; Yoo, H. Efficient Wireless Power Transfer System with a Miniaturized Quad-Band Implantable Antenna for Deep-Body Multitasking Implants. *IEEE Trans. Microw. Theory Tech.* **2020**, *68*, 1943–1953. [[CrossRef](#)]
87. Fan, Y.; Liu, H.; Liu, X.; Cao, Y.; Li, Z.; Tentzeris, M.M. Novel coated differentially fed dual-band fractal antenna for implantable medical devices. *IET Microw. Antennas Propag.* **2020**, *14*, 199–208. [[CrossRef](#)]
88. Haerinia, M.; Noghianian, S. Analysis of misalignment effects on link budget of an implantable antenna. In Proceedings of the URSI EM Theory Symposium, EMTS 2019, San Diego, CA, USA, 27–31 May 2019.
89. Aldaoud, A.; Redoute, J.-M.; Ganesan, K.; Rind, G.S.; John, S.E.; Ronayne, S.M.; Opie, N.L.; Garrett, D.J.; Praver, S. A Stent-Based Power and Data Link for Sensing Intravascular Biological Indicators. *IEEE Sens. Lett.* **2018**, *2*, 1–4. [[CrossRef](#)]
90. Li, K.R.; See, K.Y.; Koh, W.-J.; Zhang, J.-W. Design of 2.45 GHz microwave wireless power transfer system for battery charging applications. In Proceedings of the 2017 Progress in Electromagnetics Research Symposium-Fall (PIERS-FALL), Singapore, 19–22 November 2017; pp. 2417–2423.
91. Ishizaki, T.; Nishikawa, K.; Ishizaki, T.; Nishikawa, K. Wireless power beam device using microwave power transfer. In Proceedings of the 2014 IEEE Wireless Power Transfer Conference, Jeju, Korea, 8–9 May 2014; pp. 36–39.
92. Yan, X.; Zhu, Z.; Liu, G.-Q.; Zhao, X. Analysis of implantable ultrasonic coupling wireless power transmission system. *Prog. Electromagn. Res. M* **2019**, *80*, 203–214. [[CrossRef](#)]
93. Lee, S.Q.; Youm, W.; Hwang, G. Biocompatible wireless power transferring based on ultrasonic resonance devices. *Proc. Mtgs. Acoust.* **2013**, *19*, 30030. [[CrossRef](#)]
94. Kim, A.; Powell, C.R.; Ziaie, B. An Implantable Pressure Sensing System with Electromechanical Interrogation Scheme. *IEEE Trans. Biomed. Eng.* **2014**, *61*, 2209–2217. [[CrossRef](#)] [[PubMed](#)]
95. Song, S.H.; Kim, A.; Ziaie, B. Omnidirectional Ultrasonic Powering for Millimeter-Scale Implantable Devices. *IEEE Trans. Biomed. Eng.* **2015**, *62*, 2717–2723. [[CrossRef](#)]
96. Santagati, G.E.; Dave, N.; Melodia, T. Design and Performance Evaluation of an Implantable Ultrasonic Networking Platform for the Internet of Medical Things. *IEEE/ACM Trans. Netw.* **2020**, *28*, 29–42. [[CrossRef](#)]
97. Chang, T.C.; Wang, M.L.; Charthad, J.; Weber, M.J.; Arbabian, A. A 30.5 mm³ fully packaged implantable device with duplex ultrasonic data and power links achieving 95 kb/s with $<10^{-4}$ BER at 8.5 cm depth. In Proceedings of the 2017 IEEE International Solid-State Circuits Conference (ISSCC), San Francisco, CA, USA, 5–9 February 2017; pp. 460–461.
98. Meng, M.; Kiani, M. Design and Optimization of Ultrasonic Wireless Power Transmission Links for Millimeter-Sized Biomedical Implants. *IEEE Trans. Biomed. Circuits Syst.* **2016**, *11*, 98–107. [[CrossRef](#)] [[PubMed](#)]
99. Vihvelin, H.; Leadbetter, J.R.; Bance, M.; Brown, J.A.; Adamson, R.B.A. Compensating for Tissue Changes in an Ultrasonic Power Link for Implanted Medical Devices. *IEEE Trans. Biomed. Circuits Syst.* **2015**, *10*, 404–411. [[CrossRef](#)] [[PubMed](#)]
100. Lee, S.Q.; Youm, W.; Hwang, G.; Moon, K.S. Wireless power transferring and charging for implantable medical devices based on ultrasonic resonance. In Proceedings of the 22nd International Congress on Sound and Vibration, Florence, Italy, 12–16 July 2015; pp. 1–7.
101. Fang, B.; Feng, T.; Zhang, M.; Chakrabartty, S.; Biyi, F. Feasibility of B-mode diagnostic ultrasonic energy transfer and telemetry to a cm² sized deep-tissue implant. In Proceedings of the 2015 IEEE International Symposium on Circuits and Systems (ISCAS), Lisbon, Portugal, 24–27 May 2015.
102. Leadbetter, J.; Brown, J.; Adamson, R. The design of ultrasonic lead magnesium niobate-lead titanate composite transducers for power and signal delivery to implanted hearing aids. *J. Acoust. Soc. Am.* **2013**, *133*, 3268. [[CrossRef](#)]
103. Shigeta, Y.; Hori, Y.; Fujimori, K.; Tsuruta, K.; Nogi, S. Development of highly efficient transducer for wireless power transmission system by ultrasonic. In Proceedings of the 2011 IEEE MTT-S International Microwave Workshop Series on Innovative Wireless Power Transmission: Technologies, Systems, and Applications, Kyoto, Japan, 12–13 May 2011.
104. Shih, P.-J.; Shih, W.-P. Design, fabrication, and application of bio-implantable acoustic power transmission. *J. Microelectromech. Syst.* **2010**, *19*, 494–502. [[CrossRef](#)]
105. Ozeri, S.; Shmilovitz, D. Ultrasonic transcutaneous energy transfer for powering implanted devices. *Ultrasonics* **2010**, *50*, 556–566. [[CrossRef](#)]

106. Suzuki, S.-N.; Katane, T.; Saito, O. Fundamental study of an electric power transmission system for implanted medical devices using magnetic and ultrasonic energy. *J. Artif. Organs* **2003**, *6*, 145–148. [[CrossRef](#)] [[PubMed](#)]
107. Luo, B.; Long, T.; Mai, R.; Dai, R.; He, Z.; Li, W. Analysis and design of hybrid inductive and capacitive wireless power transfer for high-power applications. *IET Power Electron.* **2018**, *11*, 2263–2270. [[CrossRef](#)]
108. Barmada, S.; Tucci, M.; Raugi, M.; Dionigi, M.; Mezzanotte, P. Experimental validation of a hybrid Wireless Power Transfer-Power Line Communication system. In Proceedings of the 2016 International Symposium on Power Line Communications and its Applications (ISPLC), Bottrop, Germany, 20–23 March 2016; pp. 37–41. [[CrossRef](#)]
109. Haerinia, M.; Noghianian, S. Design of Hybrid Wireless Power Transfer and Dual Ultrahigh-Frequency Antenna System. In Proceedings of the 2019 URSI International Symposium on Electromagnetic Theory (EMTS), San Diego, CA, USA, 27–31 May 2019.
110. Meng, M.; Kiani, M. A Hybrid Inductive-Ultrasonic Link for Wireless Power Transmission to Millimeter-Sized Biomedical Implants. *IEEE Trans. Circuits Syst. II Express Briefs* **2016**, *64*, 1137–1141. [[CrossRef](#)]
111. Haerinia, M.; Noghianian, S. A Printed Wearable Dual-Band Antenna for Wireless Power Transfer. *Sensors* **2019**, *19*, 1732. [[CrossRef](#)] [[PubMed](#)]
112. Haerinia, M.; Noghianian, S. Study of Bending Effects on a Dual-Band Implantable Antenna. In Proceedings of the 2019 IEEE International Symposium on Antennas and Propagation and USNC-URSI Radio Science Meeting, Atlanta, GA, USA, 7–12 July 2019.
113. Aldaoud, A.; Redoute, J.-M.; Ganesan, K.; Rind, G.S.; John, S.E.; Ronayne, S.M.; Opie, N.L.; Garrett, D.J.; Praver, S. Near-Field Wireless Power Transfer to Stent-Based Biomedical Implants. *IEEE J. Electromagn. RF Microw. Med. Biol.* **2018**, *2*, 193–200. [[CrossRef](#)]
114. Shadid, R.; Haerinia, M.; Sayan, R.; Noghianian, S. Hybrid Inductive Power Transfer and Wireless Antenna System for Biomedical Implanted Devices. *Prog. Electromagn. Res. C* **2018**, *88*, 77–88.
115. Sharma, A.; Kampianakis, E.; Reynolds, M.S. A Dual-Band HF and UHF Antenna System for Implanted Neural Recording and Stimulation Devices. *IEEE Antennas Wirel. Propag. Lett.* **2017**, *16*, 493–496. [[CrossRef](#)]
116. Sanni, A.; Vilches, A.; Toumazou, C. Inductive and Ultrasonic Multi-Tier Interface for Low-Power, Deeply Implantable Medical Devices. *IEEE Trans. Biomed. Circuits Syst.* **2012**, *6*, 297–308. [[CrossRef](#)]
117. Wireless Medical Technologies: Navigating Government Regulation in the New Medical Age. Available online: <https://www.fr.com/files/Uploads/attachments/FinalRegulatoryWhitePaperWirelessMedicalTechnologies.pdf> (accessed on 9 November 2020).
118. Joung, Y.-H. Development of Implantable Medical Devices: From an Engineering Perspective. *Int. Neurorol. J.* **2013**, *17*, 98–106. [[CrossRef](#)]
119. Badrouchi, F.; Aymond, A.; Haerinia, M.; Selvaraj, D.F.; Tavakolian, K.; Ranganathan, P.; Eswaran, S. Cybersecurity Vulnerabilities in Biomedical Devices: A Hierarchical Layered Framework. In *Internet of Things Use Cases for the Healthcare Industry*; Raj, P., Chatterjee, J., Kumar, A., Balamurugan, B., Eds.; Springer: Cham, Switzerland, 2020.

Publisher's Note: MDPI stays neutral with regard to jurisdictional claims in published maps and institutional affiliations.



© 2020 by the authors. Licensee MDPI, Basel, Switzerland. This article is an open access article distributed under the terms and conditions of the Creative Commons Attribution (CC BY) license (<http://creativecommons.org/licenses/by/4.0/>).